Contribution of Linear and Nonlinear Processes to the Long-Term Variability of Large-Scale Atmospheric Flows

THOMAS BRUNS

Max-Planck-Institut für Meteorologie, Hamburg, F.R.G.

(Manuscript received 5 December 1984, in final form 5 June 1985)

ABSTRACT

From 10 years of Northern Hemisphere streamfunction data we estimate the contribution of linear and nonlinear processes to the variability of large-scale flow patterns at time scales up to 50 days. The dynamical model is baroclinic and quasi-geostrophic. For the horizontal and vertical representation we use spherical harmonics triangularly truncated at wavenumber 15 and the first two modes of an EOF expansion, respectively. The spectral tendency equation for each mode is formulated as a linear regression model in the frequency domain, the model quality being expressed in terms of coherence spectra. Generally two regions in wavenumber space can be distinguished, one dominated by wave propagation and the other dominated by nonlinear advection. The variance explained by these processes depends strongly on frequency and decreases toward long periods. A fraction of almost 50% streamfunction variance, integrated over large scales up to wavenumber $m = 8$, $n - m = 7$, can be explained for time scales between 2 and 14 days. For periods longer than 14 days linear propagation and nonlinear advection account for at most 30–50% observed variance for a few selected modes and about 27% of the integrated variance over all wavenumbers. For these long time periods the contributions of the internal dynamics to the long term behavior of the atmosphere cannot be meaningfully discussed without simultaneous consideration of other significant processes, such as slowly changing boundary conditions.

1. Introduction

Most atmospheric variance is contained in the largest planetary scales at low frequencies. The dynamics of these planetary flows, which also interact effectively with the ocean, is therefore of special interest for climate research. In a recent paper Egger and Schilling (1983) suggest that much of the long-term variability of the large-scale planetary flow could be explained by the nonlinear vorticity transfer from synoptic scales. Alternatively, it has been suggested from studies of idealized nonlinear spectral models with only a few degrees of freedom that for a given inhomogeneous forcing the flow might be characterized by a multiple set of quasi-stationary states (attractors), which represent analogues of observed persistent flow anomalies (Charney and DeVore, 1979; Charney and Straus, 1980). According to this theory low frequency variance of the planetary components results from occasional transitions between the attractors due to higher order instabilities (Egger, 1981; Rheinhold and Pierrehumbert, 1983), whereas the existence and structure of the attractors is essentially determined by the forcing and the nonlinear dynamics of the large scales themselves.

In this paper we test these theories by determining the correlation between the proposed internal processes and observed streamfunction changes.

The basic starting point of our study is the question of whether it is meaningful to use low-order atmospheric models for climate studies. The answer depends on how much of the observed variance can be explained by the model. Linear regression techniques are therefore applied to fit low-order models with different spectral truncations and different physics to observed streamfunction changes. The approach is described and discussed in detail by Kruse (1983) and Kruse and Hasselmann (1985) for a barotropic quasi-geostrophic model. Here we present a generalized correlation analysis of a baroclinic model in the frequency domain that provides insight into the spectral distribution of the streamfunction variance rather than just the total variance of discrete streamfunction changes.

We find that a significant fraction of atmospheric variance can be explained for short and medium time scales up to two weeks. For longer time scales the explained variance decreases strongly. Nevertheless, it cannot be concluded that long-term fluctuations are not caused by internal mechanisms, because our method becomes insensitive at low frequencies. We discuss therefore an alternative analysis method for very low frequencies.

The multiple cross-spectral analysis approach used in this paper is related to the technique first introduced by Deland (1964), and generalized and reviewed by Hayashi (1982), in which the variance contribution of propagating waves was determined from the cross-spectra of the spatial Fourier coefficients of the geopotential (section 5). The details of our method and the model strategy are described in sections 3 and 4, and results are presented in sections 6–8.

2. Dynamical equations, spatial representation and data base

Our statistical model is based on the familiar quasi-geostrophic vorticity and thermodynamic equations in pressure coordinates

$$\left.\begin{aligned} &\frac{\partial}{\partial t}\nabla^2\psi + J(\psi, \nabla^2\psi + f) - f_0\frac{\partial\omega}{\partial p} = 0 \\ &\frac{\partial}{\partial t}\frac{\partial\psi}{\partial p} + J\left(\psi, \frac{\partial\psi}{\partial p}\right) + \frac{\sigma\omega}{f_0} = 0 \end{aligned}\right\} \quad (1)$$

with vertical boundary conditions

$$\omega = \begin{cases} \rho_{\text{surf}} f_0 \dfrac{\partial}{\partial t}\psi_{\text{surf}} - \rho_{\text{surf}} g J(\psi_{\text{surf}}, h) - \epsilon\nabla^2\psi_{\text{surf}}, \\ \qquad\qquad P = P_{\text{surf}} \\ \rho_{\text{top}} f_0 \dfrac{\partial}{\partial t}\psi_{\text{top}}, \quad P = P_{\text{top}}. \end{cases}$$

Here ψ denotes the streamfunction, ω the vertical velocity, f, f_0 the Coriolis parameter, h the bottom topography, σ the static stability, ρ the air density, g the gravitational acceleration and ϵ a frictional parameter. The model is applied to the northern hemisphere. We avoid flow across the equator by a fixed wall condition

$$\psi = 0, \quad \varphi = 0.$$

Although we use spherical coordinates, the form (1) corresponds to a β-plane formulation with a constant midlatitude Coriolis parameter f_0 [we chose $f_0 = f(45°)$], except that we allow for full meridional variation of f in the horizontal vorticity advection term. This implies, for example, that temperature advection is well described in midlatitudes only, because f_0 appears in the balance equation and in the divergence term. Advection by the divergent wind is neglected, and the static stability is further assumed to be a function of pressure only. Although (1) is not strictly scale consistent for planetary scale flows, it is nevertheless the simplest possible model for describing baroclinic processes on the sphere. The stability properties of (1) on the sphere have been extensively studied by Baines and Frederiksen (1978) and Frederiksen (1978) for a two-layer formulation.

As a data base for the statistical analysis of the quasi-geostrophic model we use the 10-year data set (1967–76) of Northern Hemisphere (10–90°N) geopotential height, which was kindly made available by the German Weather Service (DWD). These were transformed into (even) spherical harmonic coefficients, truncated at wavenumber 15, by Speth and Kirk (1981). Kruse (1983) has computed streamfunction coefficients from these data using the spectral balance equation (Eliasen and Machenhauer, 1965). For the model version to be presented here we chose the largest possible rhomboidal truncation (zonal wavenumber $m = 8$, meridional wavenumber $n - m = 7$), corresponding to 68 odd spectral modes (4 zonal mean modes and $8 \times 4 \times 2$ cosine and sine wave modes). Thus, the predictands of the statistical model include both planetary ($m \leq 5$) and medium scale synoptic flows ($6 \leq m \leq 8$). However, for the predictor fields (source terms) we computed also the transfer of vorticity and heat from the remaining smaller synoptic scales out to the full triangular cutoff limit (Fig. 1).

In the vertical, four tropospheric pressure levels (850–700–500–300 hPa) are resolved. In order to reduce the number of degrees of freedom, a vertical EOF-expansion of the streamfunction anomalies from a basic-state, averaged over the hemisphere, was performed. The basic state consists of the time mean and the first harmonic of the seasonal cycle. The subtraction of the seasonal cycle is useful, since it removes some of the cyclostationary properties from the data. The model itself is formulated in terms of the anomaly fields, and the statistical analysis is then carried out assuming a time independent model and stationary statistics. Thus the nonstationary, seasonal variations of the second moments are not considered.

For the model formulation we keep only the first two modes of the EOF-expansion (Fig. 2). These already represent 99% of the hemispherically integrated anomaly variance. The EOFs exhibit a universal structure which is almost the same for all wavenumbers. A similar tropospheric EOF structure was found also by Fraedrich and Dümmel (1983) for a single station. The first mode shows the well-known equivalent barotropic structure. The second mode has a zero crossing at about 500 hPa. For brevity we shall therefore refer to the first EOF-mode as barotropic and the second as baroclinic.

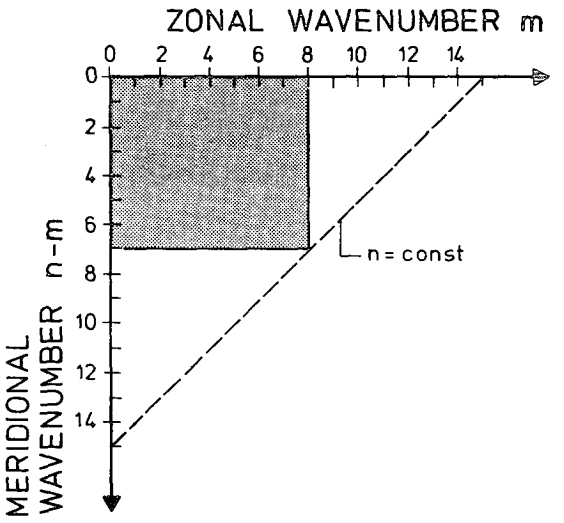

FIG. 1. Schematic representation of the rhomboidal model domain (shaded) and the triangular domain of available streamfunction data in wavenumber space. Only $n - m$ = odd spherical harmonic coefficients are used. The predictands are limited to the rhomboidal domain; the predictors are computed for the full triangular domain.

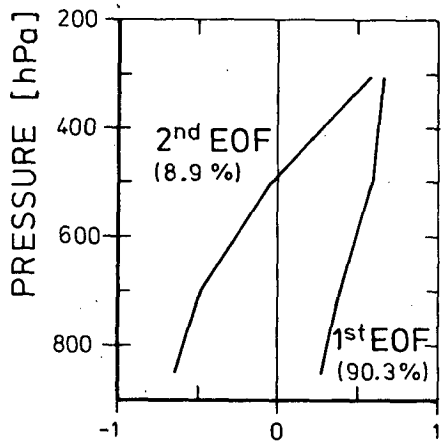

FIG. 2. First two eigenvectors of the covariance matrix of streamfunction anomalies, integrated over the hemisphere.

The two modes will actually be found to exhibit the dispersion relation properties expected for barotropic and baroclinic modes.

The spectral representation of the streamfunction finally takes the form

$$\psi(\lambda, \varphi, p, t) = \tilde{\psi}(\lambda, \varphi, p, t) + \sum_{\nu} [\sum_{k} \psi_{\nu}^{k}(t) F^{k}(p)] Y_{\nu}(\lambda, \varphi) \quad (2)$$

where $\tilde{\psi}$ is the basic state, F^k the kth vertical expansion function and Y_ν denotes the spherical harmonics in real representation. The subscript ν is a composite index identifying the sine or the cosine mode and wavenumber (m, n). Substitution of (2) into (1), elimination of the vertical velocity and projection onto each anomaly mode then yields equations of the general form

$$\dot{\psi}_{\nu}^{k} = \mathrm{BETA}_{\nu}^{k} + \mathrm{VABS}_{\nu}^{k} + \mathrm{TABS}_{\nu}^{k} + \mathrm{VADV}_{\nu}^{k} + \mathrm{TADV}_{\nu}^{k} + \mathrm{ORO}_{\nu}^{k} + \mathrm{EKM}_{\nu}^{k} \quad (3)$$

where the forcing terms on the rhs are collected in groups as follows:

BETA represents the advection of planetary vorticity, the Rossby wave β-term; VABS and TABS denote all interactions between anomalies and the seasonal vorticity and temperature fields, respectively. The effect of these two terms is mainly to modify the Rossby wave phase velocity, but interactions with the stationary waves are also included.

The VADV and TADV describe the corresponding nonlinear interactions arising from the vorticity and temperature advection terms. Finally, ORO and EKM represent the boundary effects of orographic forcing and Ekman pumping, respectively.

Since no forcing is included, the tendency equation (3) is of course not capable of describing the long-term atmospheric behavior correctly. The statistical analysis we apply is therefore purely diagnostic to overcome the accumulation of forecast errors. We note, however, that the neglect of forcing reduces the explained variance, particularly for the zonal mean modes which depend very much on diabatic heating.

The terms carry coefficients, which depend in detail on the form of the vertical EOFs. For our purposes the exact calculation of these coefficients is irrelevant, since we shall regard the terms on the rhs as predictors whose coefficients will be determined empirically to optimize the simulation of the lhs predictand. This will be carried out for each frequency band separately, so that the coefficients will in effect be determined as a function of frequency.

The model bottom topography (based on GFDL data described by Smith *et al.*, 1965), is triangularly truncated at wavenumber 15. However, orographic effects are probably inadequately represented, since mountains are treated as small deviations from a plane, whereas the real topography can extend high into the model domain. The use of σ-coordinates, rather than pressure coordinates, would reduce this problem but would also require a nongeostrophic formulation of the model to represent the orographic forcing appropriately.

3. The statistical formulation

We are interested primarily in the specific contributions of the various terms on the rhs of (3) to the observed change of the streamfunction, rather than in the overall performance of the model. Therefore, instead of integrating (3) from some initial value and comparing the final field with observations in the traditional manner, we consider the correlation between each individual term and the observed streamfunction tendency. Since the different physical processes do not act uniformly over all time scales a frequency dependence is to be expected. We therefore formulate the regression model in the frequency domain

$$i\omega \Psi_{\nu}^{k}(\omega) = \sum_{j=1}^{p} H_{\nu j}^{k}(\omega) Z_{\nu j}^{k}(\omega) + R_{\nu}^{k}(\omega), \quad (4)$$

where the Fourier coefficient $i\omega\Psi$ of the streamfunction tendency is the predictand, and the Fourier coefficients Z of the terms on the rhs of (3) represent the predictors, R denoting the residual. The complex transfer functions H are regarded here as empirical regression coefficients which are determined by minimizing the residual variance (see Jenkins and Watts, 1968),

$$H_j(\omega) = i\omega \sum_{i=1}^{p} \Gamma_{i,j}^{*-1}(\omega) \Gamma_{i,p+1}(\omega), \quad (5)$$

where Γ is the $(p+1) \times (p+1)$ cross-spectral matrix of the p predictors and the streamfunction $(p+1)$ and Γ^* is the $p \times p$ cross-spectral matrix of the predictors only. For convenience, the wavenumber subscripts ν, k have been dropped. The transfer functions will gen-

erally deviate from unity due to neglected processes and errors in the predictors.

The fraction of variance (skill) explained by the model is given by the multiple squared coherence $\mathscr{H}^2$, i.e., the coherence between the full model and the predictand

$$\mathscr{H}^2 = 1 - \frac{|\Gamma|}{\Gamma_{p+1,p+1}\Pi_{p+1,p+1}}, \tag{6}$$

where $\Pi_{k,m}$ denotes the minor of the element (k, m) of Γ. The absolute variance explained by the model is accordingly

$$\sigma^2 = \mathscr{H}^2\Gamma_{p+1,p+1}. \tag{7}$$

The individual coherence $\mathscr{H}_j$ between a single predictor and the predictand, and the corresponding variance σ_j^2 explained by a one-predictor-model are obtained from equations (6) and (7), by setting $p = 1$.

In addition we are interested in the partial contribution of a certain predictor to the total model variance

$$\hat{\sigma}_j^2 = \hat{\mathscr{H}}_j^2\Gamma_{p+1,p+1} \tag{8}$$

where the partial coherence $\hat{\mathscr{H}}_j^2$ defines the increase of skill resulting from the introduction of the jth predictor into the model, after all other predictors have already been included. One finds

$$\hat{\mathscr{H}}_j^2 = (1 - \mathscr{H}^2)\left(\frac{\Pi_{p+1,p+1}\Pi_{j,j}}{\Pi_{p+1,j}^2} - 1\right)^{-1}. \tag{9}$$

The partial and individual coherence are equal if the predictors are uncorrelated, but in general they will differ, either inequality being possible, depending on the form of correlation among the predictors.

We note that our modeling approach will fail in the limit of very small frequencies. In this case the predictand approaches zero and the set of predictors sum to a very small residual, which is easily masked by noise. We discuss an alternative analysis for small frequencies in section 8.

4. Model strategy

The statistical model was applied to the 10-year data set in two steps. To reduce the computational effort we first performed a linear regression analysis in the time domain (at zero time lag) in order to select the most important predictors. In this analysis, following the method of Kruse (1983), the predictands are defined as the streamfunction changes over a finite time interval of the order of days. The predictors are averaged over the same interval. In the frequency domain this corresponds to a multiplication of the Fourier coefficients by a spectral filter and the estimated regression coefficients then represent weighted frequency averages of the transfer functions.

The simpler time domain analysis enables the incorporation of a large number of predictors, and some of the terms in (3) were therefore subdivided. For example, VADV was separated into different contributions representing purely barotropic mode, purely baroclinic mode or mixed interactions. By selection and combination, the number of predictors was then successively reduced to a minimum set, which was still able, however, to reproduce most of the full model tendency variance, typically 90–95%. The results of the time domain model are presented in detail in Bruns (1985).

We discuss here only the second step: the application of the frequency domain model (5) to the remaining most significant predictors. These consist of a linear and two nonlinear terms for each of the vertical modes, which we abbreviate as LIN1, VA11 and VAEX for the barotropic mode, and as LIN2, TA12 and TAEX for the baroclinic mode.

The LIN-terms represent superpositions of all linear advection terms in (3), namely BETA, VABS and TABS, which were found to be strongly correlated among themselves. We define VA11 and VAEX as the nonlinear vorticity advection of the first mode anomalies; the first covering internal interactions within the rhomboidal truncation, the second the vorticity transfer from the remaining modes in the triangular region outside the rhomboidal region. Similarly, TA12 and TAEX denote the analogous temperature advection terms.

Our strategy of first defining a reduced model with the help of the time domain regression analysis bears the inherent danger that some potential predictive information of individual processes, which could appear only in certain frequency bands, might be lost by the spectral averaging associated with the time domain analysis. However, the relatively smooth frequency dependence of the coefficients obtained in the later, more general, spectral approach indicates that the collection of terms derived from the time domain analysis is meaningful also in the spectral domain.

5. Relation to space–time spectral analysis

Following Hayashi's (1971) analysis we may represent the variance of large-scale atmospheric flow as a composition of eastward (progressive) and westward (retrogressive) traveling waves and standing waves, where each component is assumed to be incoherent with the others due to different physical origins. By means of space–time spectral analysis the observed variance can be decomposed into the contributions of the various flow types. In particular Hayashi showed that the quadrature spectrum represents the variance difference between progressive and retrogressive waves.

Our cross-spectral analysis between the tendency of the streamfunction spherical harmonic coefficients and the terms of the model equation (3) may be regarded as a special case of space–time spectral analysis, where the model terms explicitly represent the physical origins

of the different flow types. Since our dynamical model is first order in time and contains in the simplest form only linear terms relating the sine and the cosine modes in accordance with the β-term and the zonal mean wind advection term, it can simulate only a single traveling wave, either retrograde or progressive. Space–time spectral analysis is, however, based on kinematic principles, which allow for wave propagation in either direction.

It is known from theory and observations (Eliasen and Machenhauer, 1969) that the β-effect dominates for the very long retrogressive barotropic waves, while the shorter waves travel progressively due to the mean wind advection. In between there exists a region of very slow (quasi-stationary) waves, where the two effects cancel. If only BETA is included in our statistical model the effect of the mean wind advection is projected onto BETA. The transfer function is then interpreted as a correction of the theoretical Rossby wave frequency for a best-fit model describing the β-effect alone.

Note that we have a separate model equation (3) for the sine and the cosine mode of each wavenumber:

$$\dot{\psi}_c = \mathrm{BETA}_c = \omega_0 \psi_s$$
$$\dot{\psi}_s = \mathrm{BETA}_s = -\omega_0 \psi_c, \qquad (10)$$

where ω_0 is the theoretical wave frequency. For a zonally invariant description of zonal wave propagation it would be necessary to demand equal transfer functions for the two modes. This condition, which we do not impose in our full model, is automatically fulfilled in the pure BETA-model (In this case the cross spectrum between the tendency and BETA is simply proportional to the cross spectrum between the sine and the cosine mode).

However, the condition of zonal invariance is violated if we extend the model by inhomogeneous terms that are possibly correlated with BETA. In this case the sine and cosine mode transfer functions are not necessarily equal and the variance explained by BETA cannot be interpreted formally as completely due to wave propagation in a single direction, but contains a small admixture of standing waves and waves of opposite direction. In practice these corrections are very small and our model is found to be closely zonally symmetric.

The dynamical model contains a linear feedback in the form of Ekman pumping. It seems reasonable to include such a term in the regression model in order to explain the stationary response to external forcing. However, care must be taken in introducing this term in the frequency domain. Consider a physical system Y with linear feedback

$$\dot{y} = -\epsilon y + F, \qquad (11)$$

where F is any process acting as an external forcing on the system. The corresponding frequency domain model reads

$$i\omega Y(\omega) = H_1(\omega)Y(\omega) + H_2(\omega)F(\omega). \qquad (12)$$

Obviously the feedback term is trivially coherent with the predictand. Thus, if the transfer function is allowed to become imaginary a linear feedback term results in a singular cross-spectral matrix. However, under the condition that the transfer function is real it is possible to include such a term and determine the feedback parameter.

In our frequency domain model, where complex transfer functions are considered, a linear feedback was not included, because the EKM-term was found to be of minor significance in the time domain analysis. However, the effect of linear feedback is projected onto the transfer functions of the other terms. For example, the solution of (11) is given by

$$Y(\omega) = F(\omega)(\epsilon + i\omega)^{-1},$$

and therefore a regression model (12) without linear feedback would yield a biased transfer function

$$H_2(\omega) = i\omega(\epsilon + i\omega)^{-1},$$

indicating a phase shift between the tendency and the forcing, which in reality does not exist. Conversely, if no phase shift is found in the transfer function we may conclude that the neglect of linear feedback was reasonable.

6. Examples of coherence spectra and transfer functions

For the frequency domain analysis the 10-year time series was divided into 73 segments of 50 days length, yielding 146 degrees of freedom for the spectral estimates. For a comparison, the cross spectra were also estimated by averaging over frequency bands, but no significant differences were found.

Figure 3 shows four examples of coherence spectra of the three predictors LIN1, VA11 and VAEX for different meridional wavenumbers of the barotropic ($m = 1$) cosine mode. The thick solid line in each panel is the multiple squared coherence $\mathscr{R}^2$ of the full model including all three predictors. The broken and solid thin lines represent the partial coherence $\hat{\mathscr{R}}_j^2$ and individual coherence $\mathscr{R}_j^2$, respectively.

The contributions of LIN1 decrease with increasing meridional wavenumber. Since this predictor mainly represents zonal wave propagation, we will term those modes quasi-stationary for which the LIN1-coherence is close to zero. The high coherence of LIN1 extends over a relatively wide frequency range, presumably because the normal mode Rossby waves (Ahlquist, 1982) are not exactly represented by single spherical harmonic modes. The seasonal dependence of the basic flow might also have a similar effect by varying the Rossby wave frequency. The contributions of the nonlinear vorticity advection terms appear to be most important for the quasi-stationary modes. The external interac-

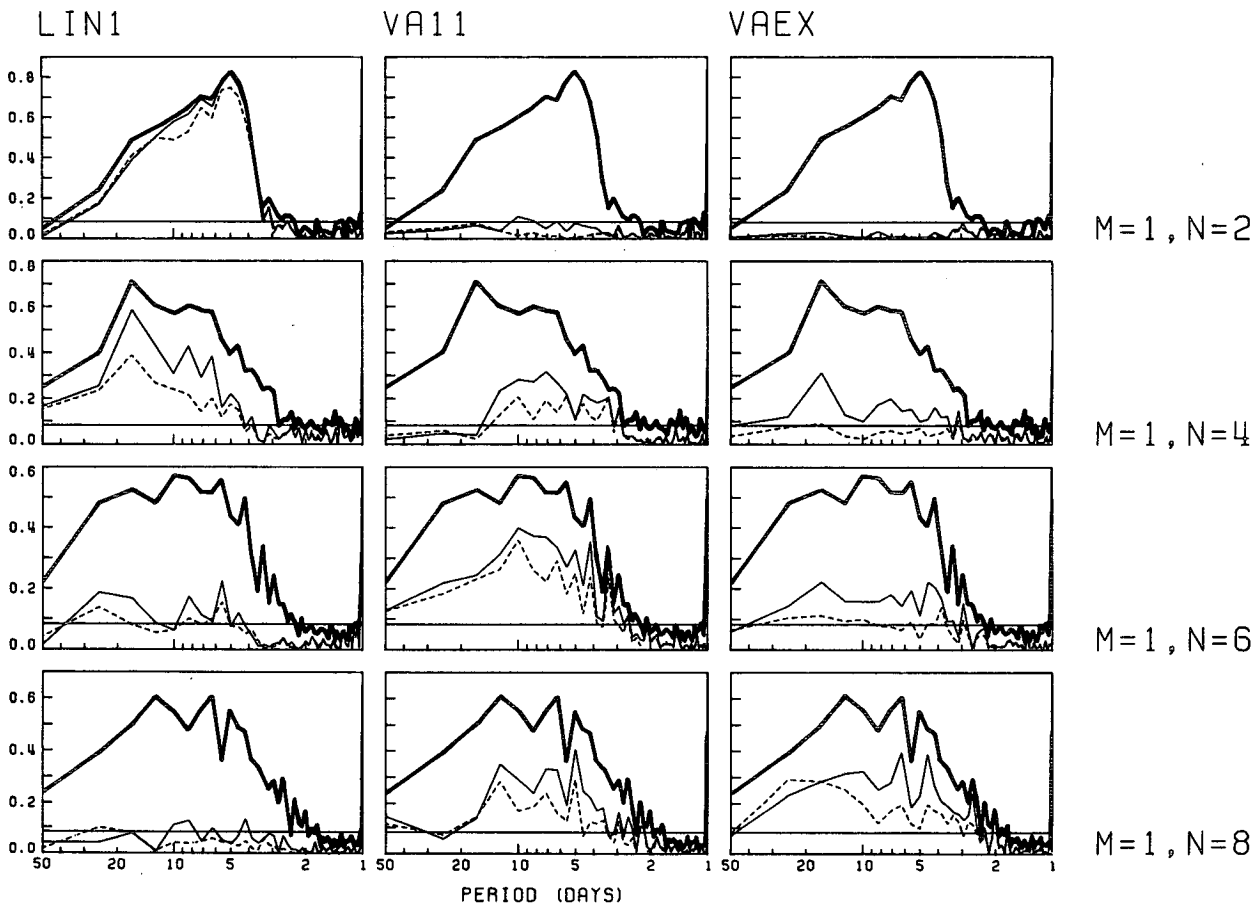

FIG. 3. Examples of coherence spectra between the barotropic streamfunction mode and the three predictors LIN1, VA11, VAEX from left to right. The thick solid line in each frame is the multiple squared coherence $\mathscr{R}^2$ of the full model including all three predictors. The broken and solid thin lines represent partial coherence $\hat{\mathscr{R}}_j^2$ and individual coherence $\mathscr{R}_j^2$, respectively.

tions (VAEX) are comparable in significance with the internal interactions (VA11). Another important result is the relatively low coherence at low frequencies, although in some cases this exceeds the 95% confidence limit of the null hypothesis even for the longest period resolved (50 days). For periods shorter than 2 days the coherence is always insignificant. This general frequency dependence is found for all wavenumbers. The relatively small difference between individual and partial coherence indicates that the three predictors are approximately, although not completely independent.

Figure 4 shows comparisons between observed streamfunction spectra and spectra of the model residual. Both have a pronounced red noise characteristic. The significant peak in the mode $n - m = 1$ at a period of 5 days seems to be well explained by LIN1, since the residual spectrum no longer has a peak at this frequency. The existence of a global scale 5-day wave has already been reported by other authors; see, for example, Madden and Julian (1972), Madden (1979), Ahlquist (1982).

Finally, we consider the transfer functions in Figs. 5 and 6. In all examples the amplitudes (Fig. 5), as well as the coherence, decrease systematically toward low frequencies, instead of scattering erratically.

However, it is encouraging that the amplitudes of Fig. 5 scatter around the theoretical value 1 at frequencies for which the coherence is significant. In all of these cases the corresponding phase (Fig. 6) scatters around zero, which seems to indicate that linear feedback does not play a significant role.

7. Wavenumber dependence of model variance

To obtain an overview of all predictands, we consider in this section the distribution of model variance in wavenumber space, averaged over three frequency bands:

long periods	14–100 days	(Fig. 7)
medium periods	8–14 days	(Fig. 8)
short periods	2–8 days	(Fig. 9).

Figures 7–9 show the variance distribution for the barotropic mode [Eqs. (8), (9)]. The maximum of about 50% explained variance for the long periods (top left panel, Fig. 7), in which we are especially interested, is

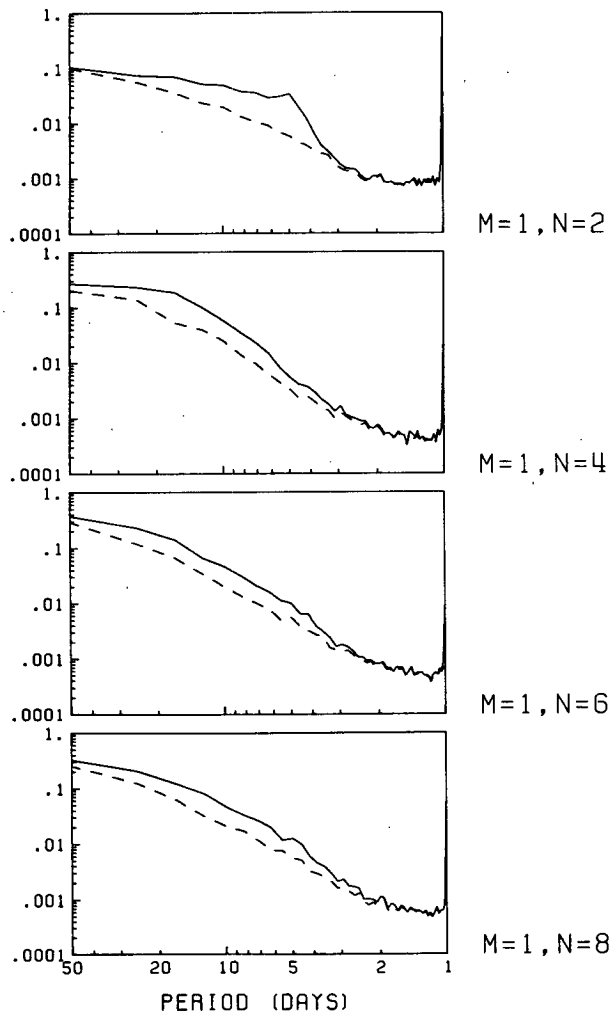

FIG. 4. Variance spectra of the observed streamfunction and the full model residual (broken line) corresponding to Fig. 3 (arbitrary units).

found at wavenumber $m = 1$, $n - m = 3$. For medium and short periods the coherence values are generally larger (up to 80%) and concentrated in two regions, the ultralong and the medium synoptic scales.

This structure is consistent with the variance patterns of LIN1. The variance explained by LIN1 is generally about the same for the sine and the cosine mode of each wavenumber. This supports the interpretation that LIN1 mainly represents wave propagation and that the inhomogeneous contributions from interactions with the basic state are quite small. Therefore, large values indicate propagating modes; the upper left region of the box representing westward traveling, and the lower right eastward traveling modes. Between these we find a region of quasi-stationary modes (around $n = 7$). Since the transfer function phases are zero in all cases, the direction of propagation is given by the theoretical wave frequency according to the superposition of the mean wind advection and the β-effect. Note also that the variance of the zonal mean modes ($m = 0$) cannot be explained by LIN1. The position of the maximal explained variance depends on the specific frequency interval. For long periods LIN1 explains most of the variance of the slowly traveling waves, which in wavenumber space are located close to the quasi-stationary region. With increasing frequency both variance maxima move away from this region to the fast traveling modes. For any given period interval the variance maximum always lies at the wavenumbers corresponding to the freely propagating waves of that period.

It is striking that for the nonlinear terms VA11 and VAEX large values of partial, as well as individual, variance are predominantly located in the quasi-stationary gap, which slightly broadens as the frequency increases. Maxima occur at meridional wavenumber $n - m = 5$ for VA11 and at $n - m = 7$ for VAEX and are approximately of the same magnitude, ranging from 18% at long periods to 29% at medium periods.

At first sight the patterns of partial and individual variance look quite similar for each of the predictors, indicating that the three predictors are approximately uncorrelated. However there are some exceptions. For short periods all three predictors are correlated, particularly for the shorter wavelengths.

For the baroclinic mode similar results are obtained, except that here all modes travel eastward. Variances are shown for the medium and short periods only (Figs. 10 and 11). The quasi-stationary modes have zonal wavenumber $m = 1$; the average phase velocity of the shorter waves increases with increasing m. The nonlinear temperature advection terms TA12 and TAEX are strongly correlated with LIN2 and significant partial variance is therefore found only for the quasi-stationary modes. For long periods (not shown) the partial as well as the individual variance patterns of TA12 and TAEX are somewhat erratic. The corresponding coherences seldom exceed the 95% significance level.

Figure 12 displays the percentages of explained variance integrated over all wavenumbers for both vertical modes, taking into account the wavenumber dependence of variance. In general the linear terms give the strongest contribution to the full model variance, which is almost 50% of the observed variance at medium and short periods, but only half as much at long periods. The two nonlinear vorticity advection terms together account for about 15–20% of the observed barotropic variance at all time scales. Since the contributions of these terms are of comparable magnitude, an improvement can be expected if data of smaller scales than wavenumber 15 were included in our analysis. The degree of correlation between the terms increases with frequency.

8. Low frequency behavior

If the processes included in our model (3)–(5) described the evolution of the streamfunction exactly, the total coherence would be unity and we would also

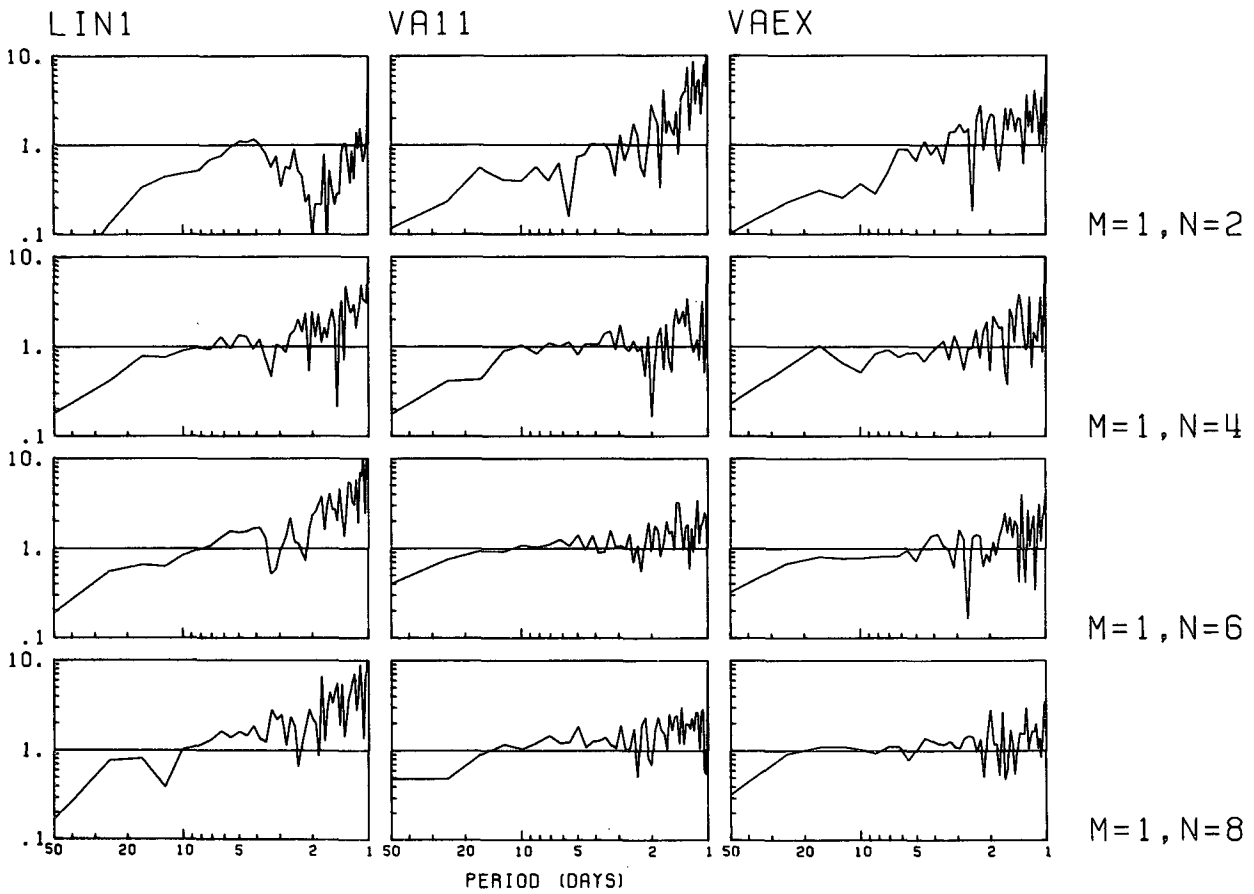

FIG. 5. Amplitude of the transfer functions corresponding to Fig. 3.

obtain transfer functions $H(\omega) = 1$, provided the coefficients of the terms were evaluated correctly. In the regions of high coherence for medium and high frequencies, we do indeed find transfer functions near unity. However, for low frequencies, both the coherence and the transfer functions drop off strongly (cf. Figs. 3 and 5).

This low-frequency behavior may be explained by the fact that the predictand, the streamfunction tendency, is proportional to ω and therefore approaches zero as $\omega \rightarrow 0$. Theoretically, the predictors should therefore sum to almost zero for low frequencies. However, in the presence of noise the small residual is masked, and the coherence becomes small. If the errors consisted of purely uncorrelated additive noise, the predictors themselves being error free, the transfer functions would still be determined correctly as unity. However, in the more realistic case that the predictors themselves also contain noise, both the coherence and the transfer functions decrease as $\omega \rightarrow 0$, in accordance with our results (cf. Figs. 3 and 5).

To test the model at low frequencies it is perhaps more appropriate to determine whether the three predictors do indeed sum to approximately zero, rather than try to correlate the individual predictors against an almost vanishing signal. For this purpose we may attempt to find a linear combination of the predictors

$$R = \sum_{j=1}^{p} h_j Z_j, \tag{13}$$

whose low-frequency variance is small compared to the variance of the terms themselves. To determine the coefficients h_j we therefore minimize the function

$$\lambda = \frac{\langle R^2 \rangle}{\sum_j \langle Z_j^2 \rangle h_j^2} = \frac{\sum_k \sum_j \langle Z_j' Z_k' \rangle h_j' h_k'}{\sum_j h_j'^2} \overset{!}{=} \min, \tag{14}$$

where the normalization $Z_j' = Z_j / \langle Z_j^2 \rangle$, $h_j' = h_j \langle Z_j^2 \rangle$ has been introduced. The angle brackets denote the expected values at zero frequency. Here, we consider the covariance of the predictors averaged over the 50-day segments. Differentiation of (14) with respect to the coefficients h_j' yields the eigenvalue problem

$$\sum_j [\langle Z_j' Z_i' \rangle - \lambda \delta_{ij}] h_j' = 0. \tag{15}$$

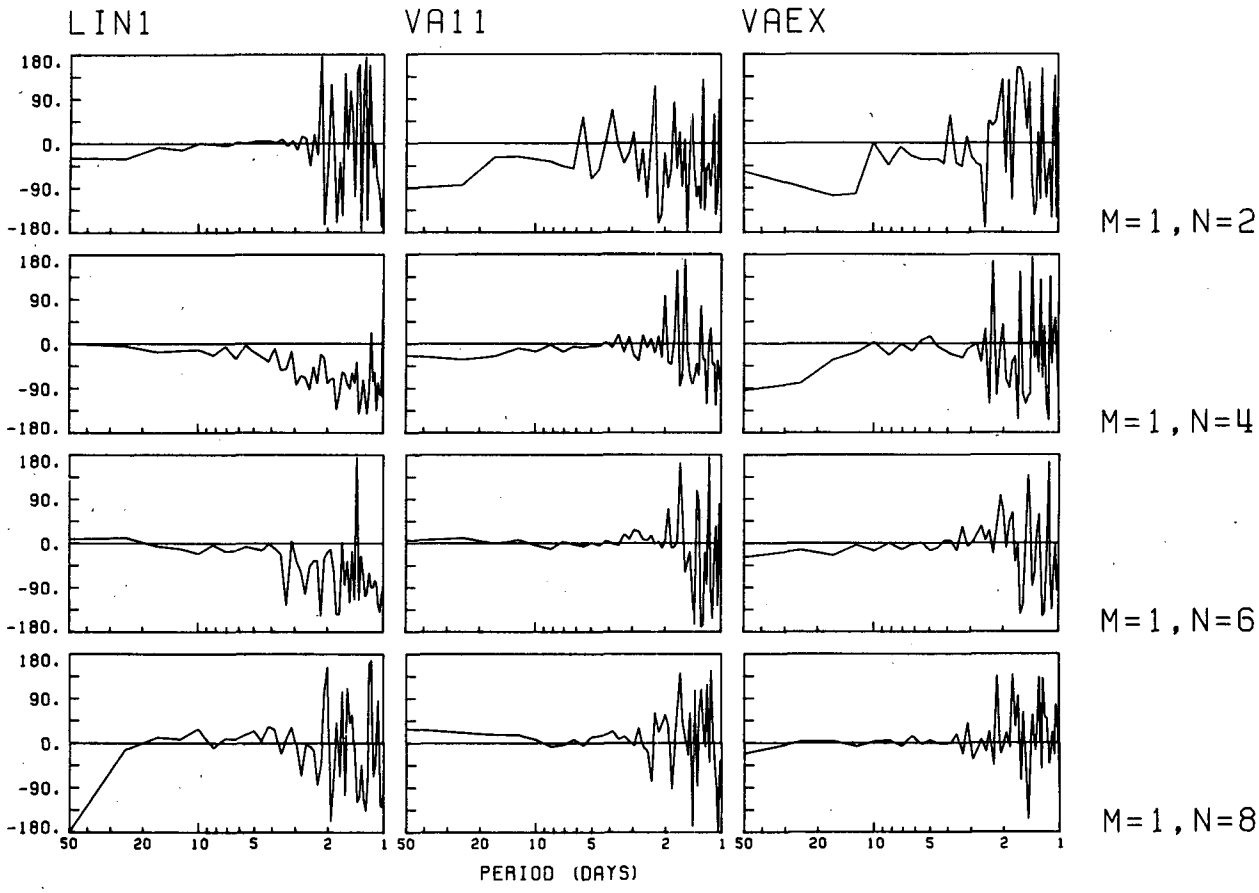

FIG. 6. Phase of the transfer functions corresponding to Fig. 3.

It follows from (14) that λ must be the smallest eigenvalue of the correlation matrix and h_j' the corresponding eigenvector. For physically realistic values the unnormalized coefficients h_j should be of the same sign and order of magnitude since for the original model, unmodified by regression, $h_j = 1$. Thus the balance can only be achieved if the terms are negatively correlated.

Figure 13a shows the barotropic mode wavenumber distribution of λ if the coefficients h_j are indeed set equal to unity. Relatively small values ($\sim$30%) are found predominantly in the region of the progressive wave modes ($n > 7$), whereas in the zonal mean and the first meridional modes the sum of terms exhibits a large variance comparable with the variance of the individual terms.

The results of the minimization of λ are shown in Fig. 13b. The wavenumber dependence of the smallest eigenvalue is almost the same as in Fig. 13a, but the absolute values are smaller by a factor of 3. In most cases the corresponding coefficients h_j are realistically positive for all three terms, although they are not always of the same order of magnitude.

For the progressive wave modes whose characteristic time scales of fluctuation is relatively small (<10 days), a low-frequency balance between the terms, mainly LIN1 and VA11, seems to be well achieved. The terms tend to balance also in the quasi-stationary region, although here the eigenvalues are larger.

In the regions of large λ, however, no realistic linear combination of terms with small variance can be found. We conclude that in these regions the low-frequency variability cannot be satisfactorily accounted for alone by the terms included explicitly in the model, and that the terms must therefore be balanced by external forcing, such as the nonresolved eddy fluxes or surface heating.

9. Conclusions

The vertical decomposition into EOFs captures 99% of the variance and separates the streamfunction field into two dynamically essentially independent modes, which exhibit the linear propagation properties expected for a barotropic and first baroclinic mode.

At all time scales we observe a clear separation of wavenumber space into two regions, one dominated by wave propagation, the other dominated by nonlinear advection. The propagating modes appear to be only

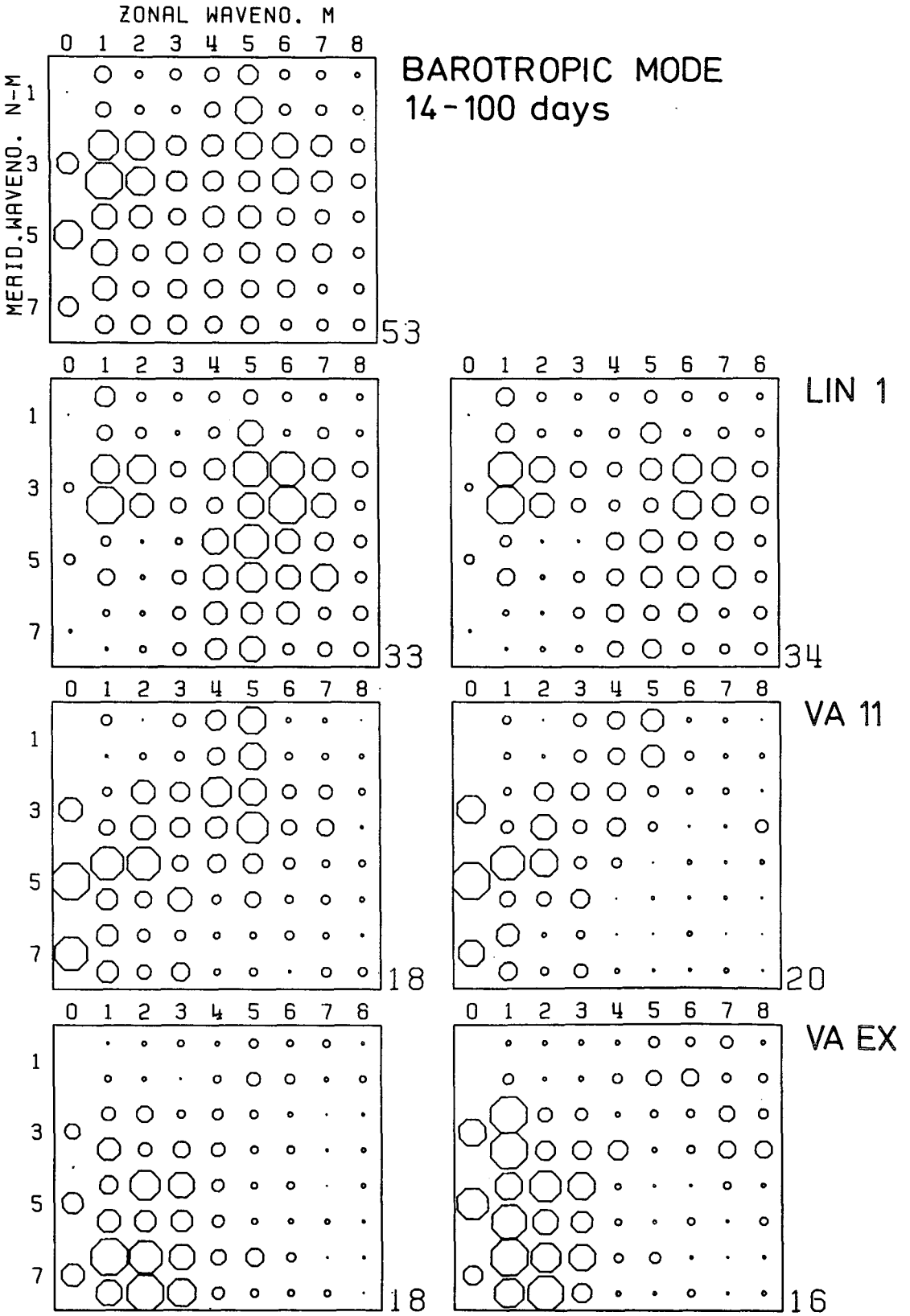

FIG. 7. Wavenumber representation of the relative variance explained by the model for the barotropic mode, integrated over long periods (14–100 days). For each wavenumber $m \neq 0$ and odd $n - m$ there are two octagons, the upper and lower representing the cosine and the sine mode, respectively. The small numbers represent the maximum value in % for each frame. The uppermost panel shows the distribution for the full model, the others show the partial (left) and individual (right) contributions of each predictor.

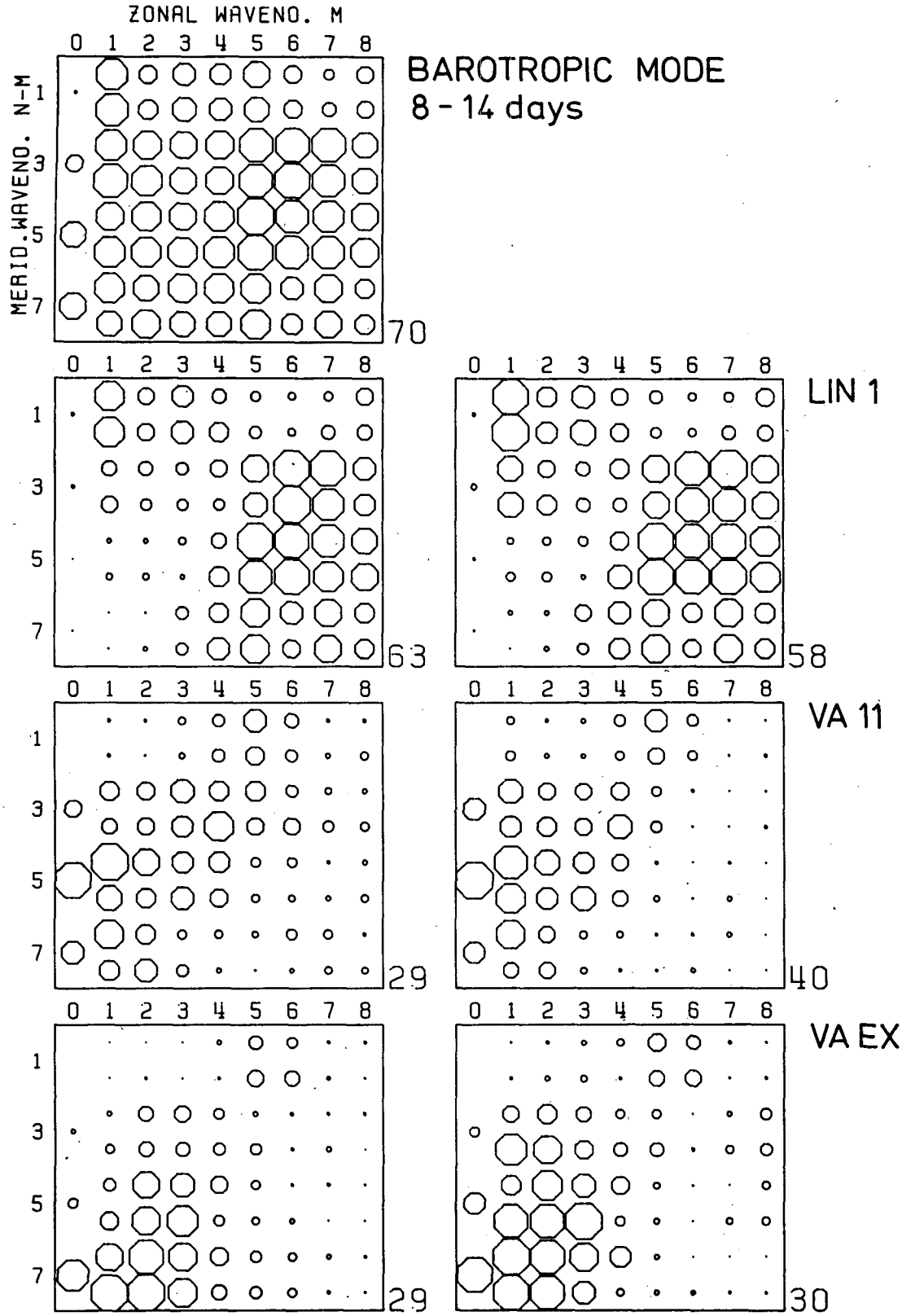

FIG. 8. As in Fig. 7 but integrated over medium periods (8–14 days).

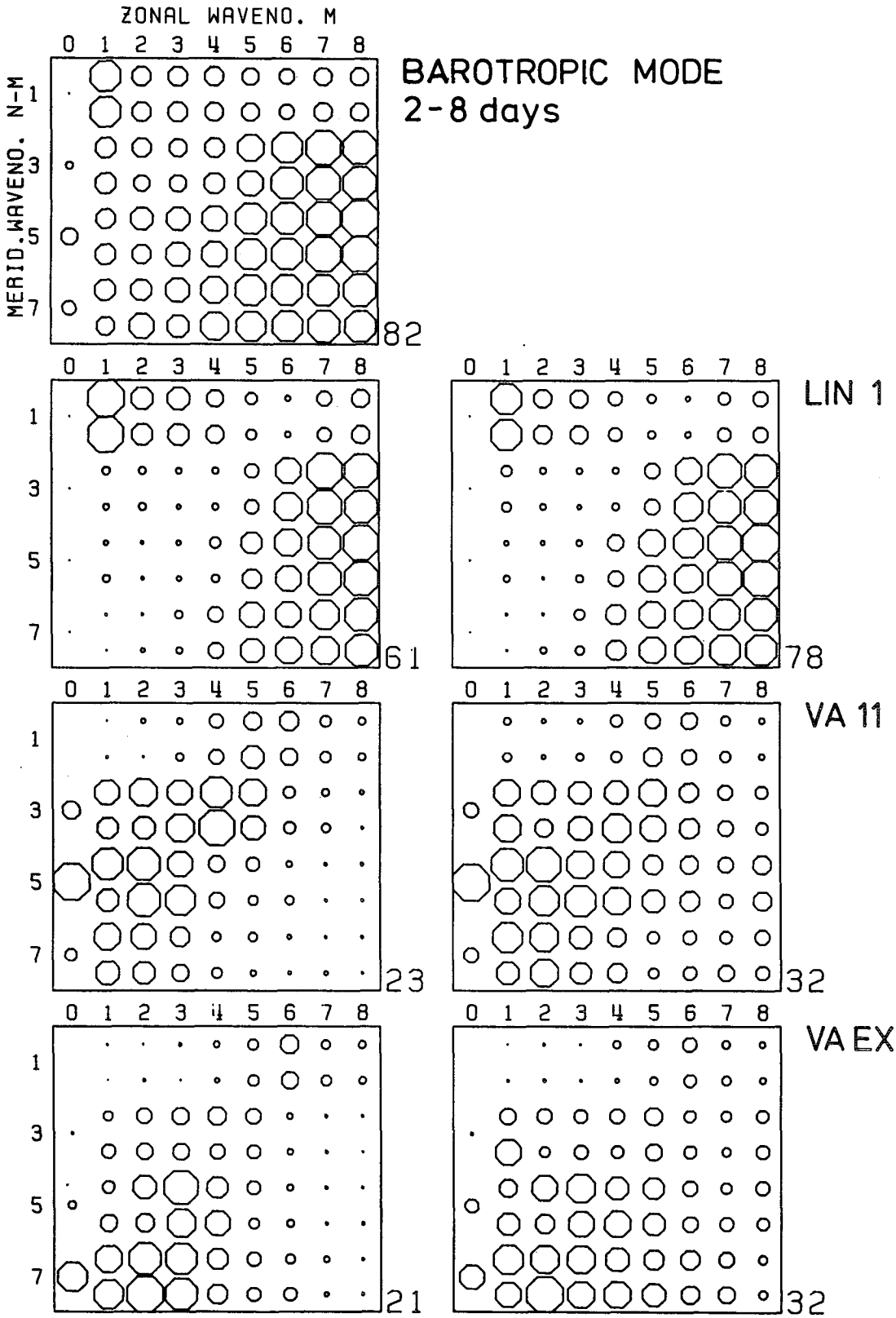

FIG. 9. As in Fig. 7 but integrated over short periods (2–8 days).

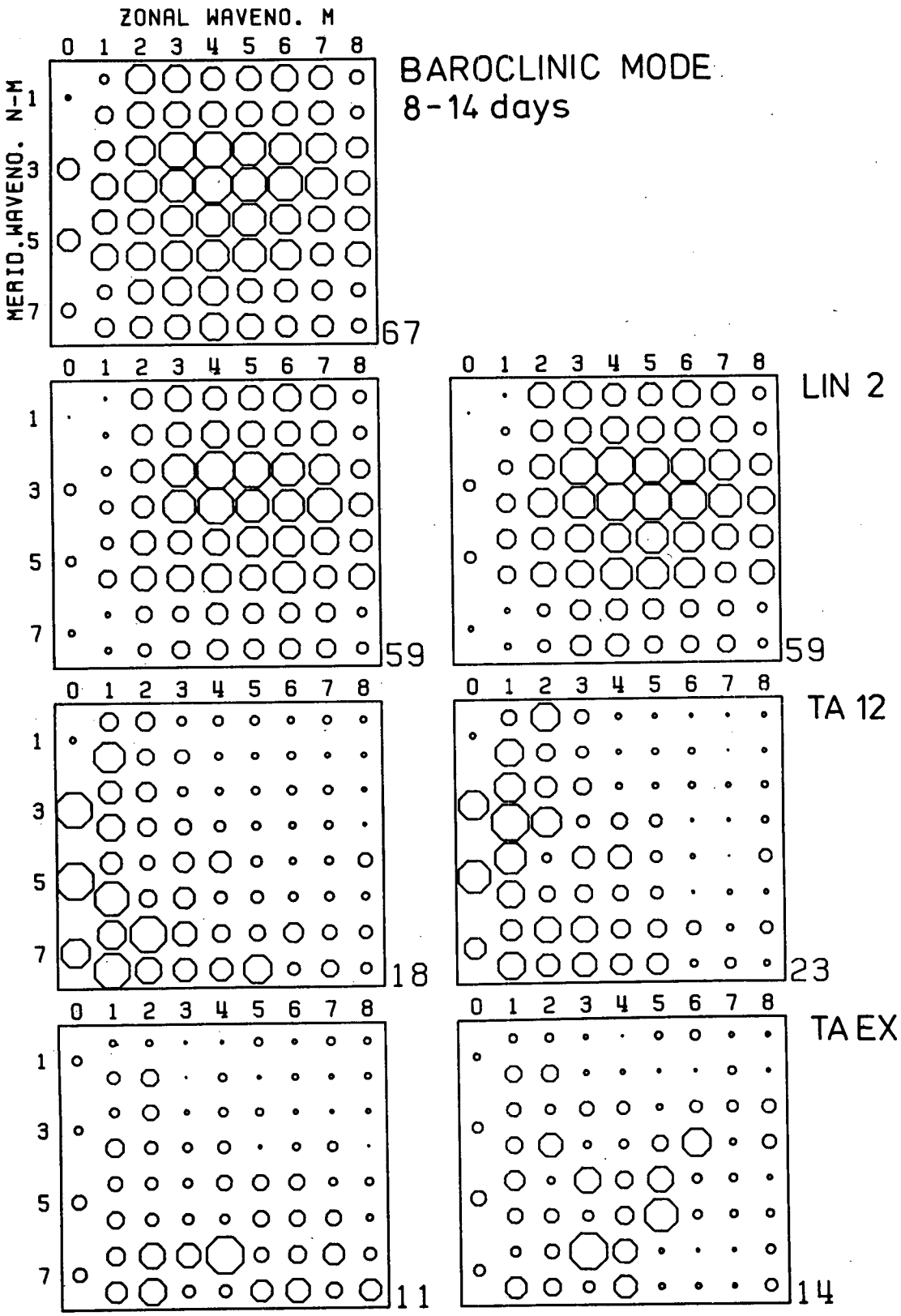

FIG. 10. As in Fig. 7 but for the baroclinic mode, integrated over medium periods (8–14 days).

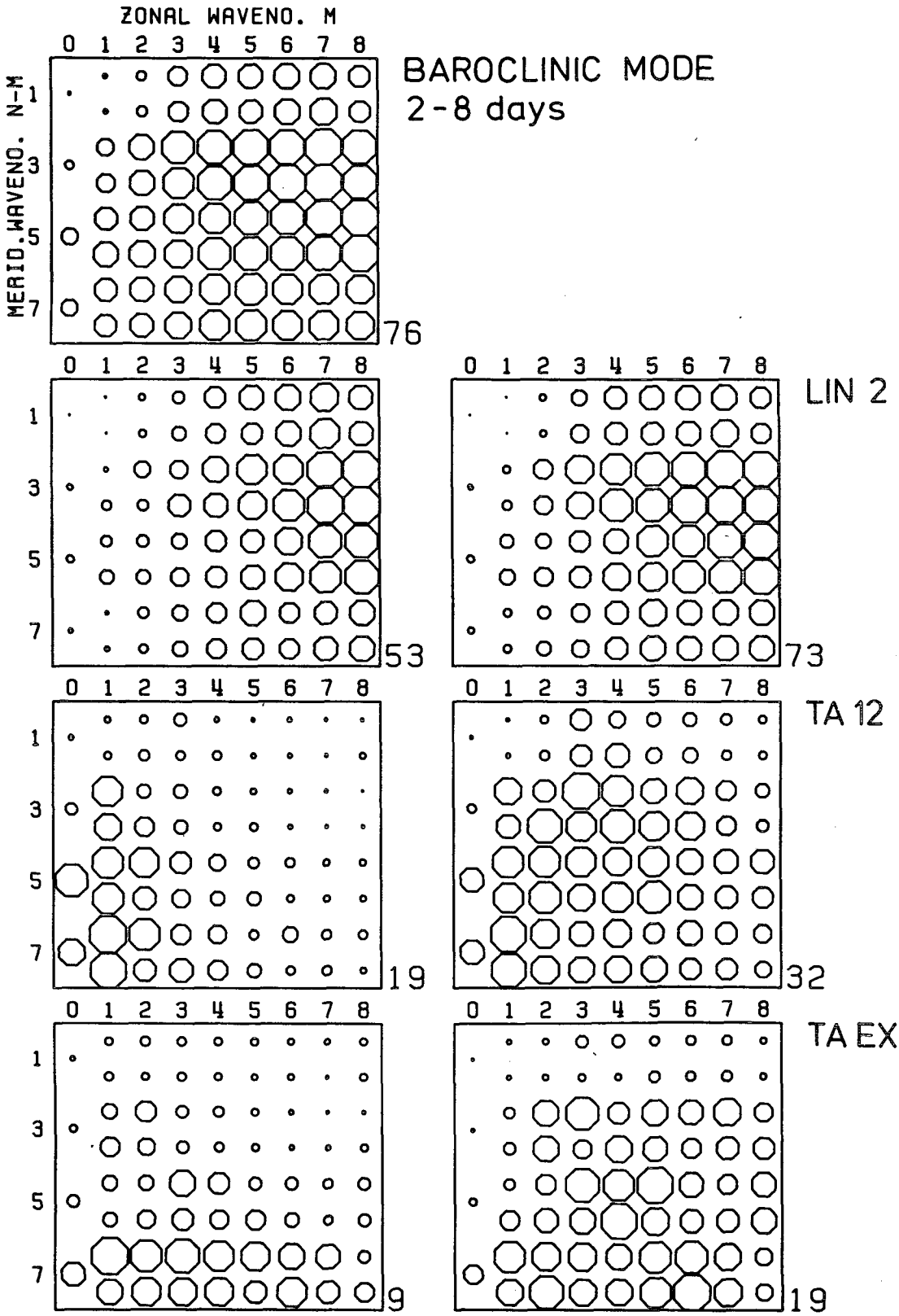

FIG. 11. As in Fig. 10 but integrated over short periods (2–8 days).

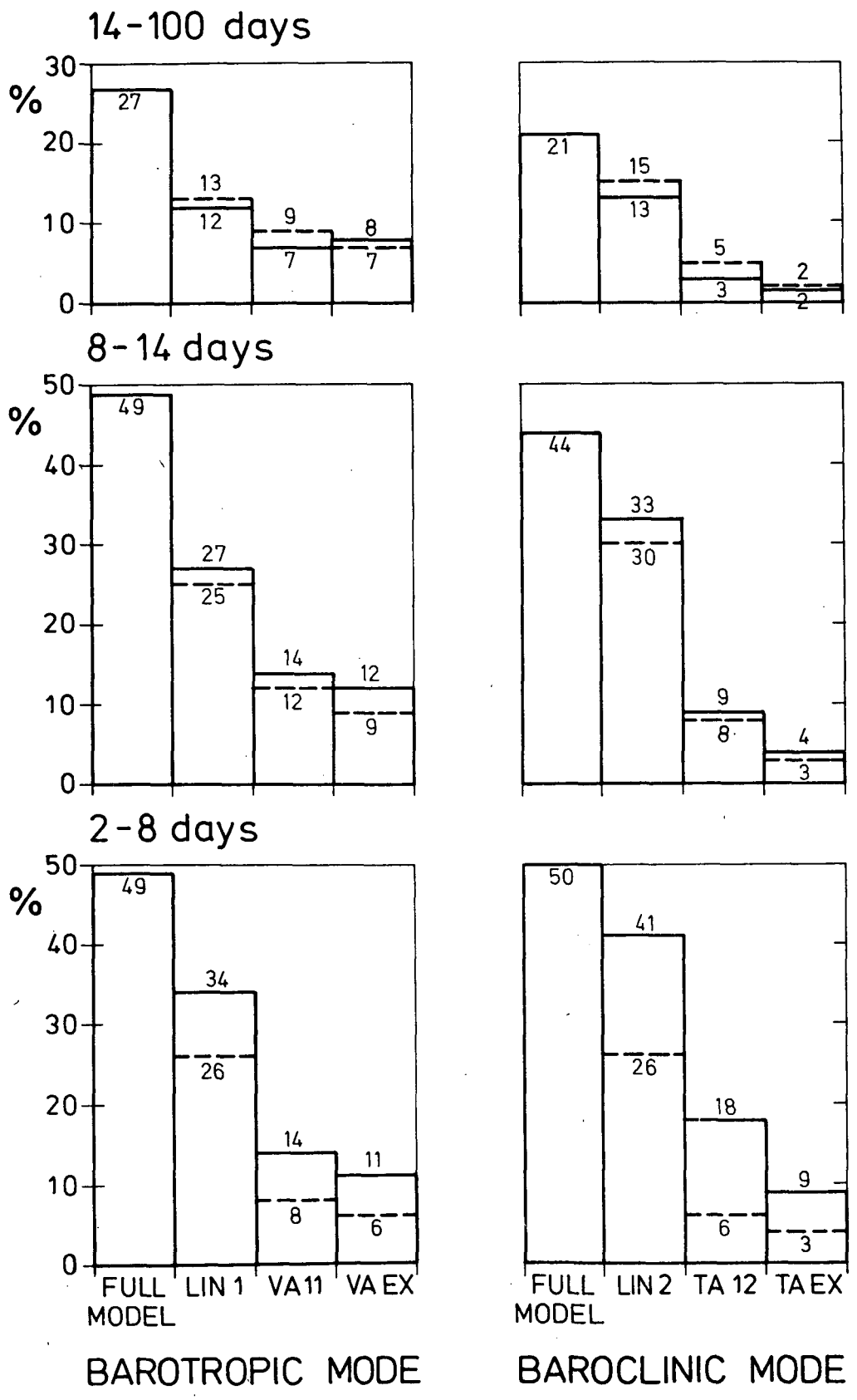

FIG. 12. Percentage of observed variance that is explained by the model, integrated over all wavenumbers and different periods. Partial variance is denoted by the broken lines.

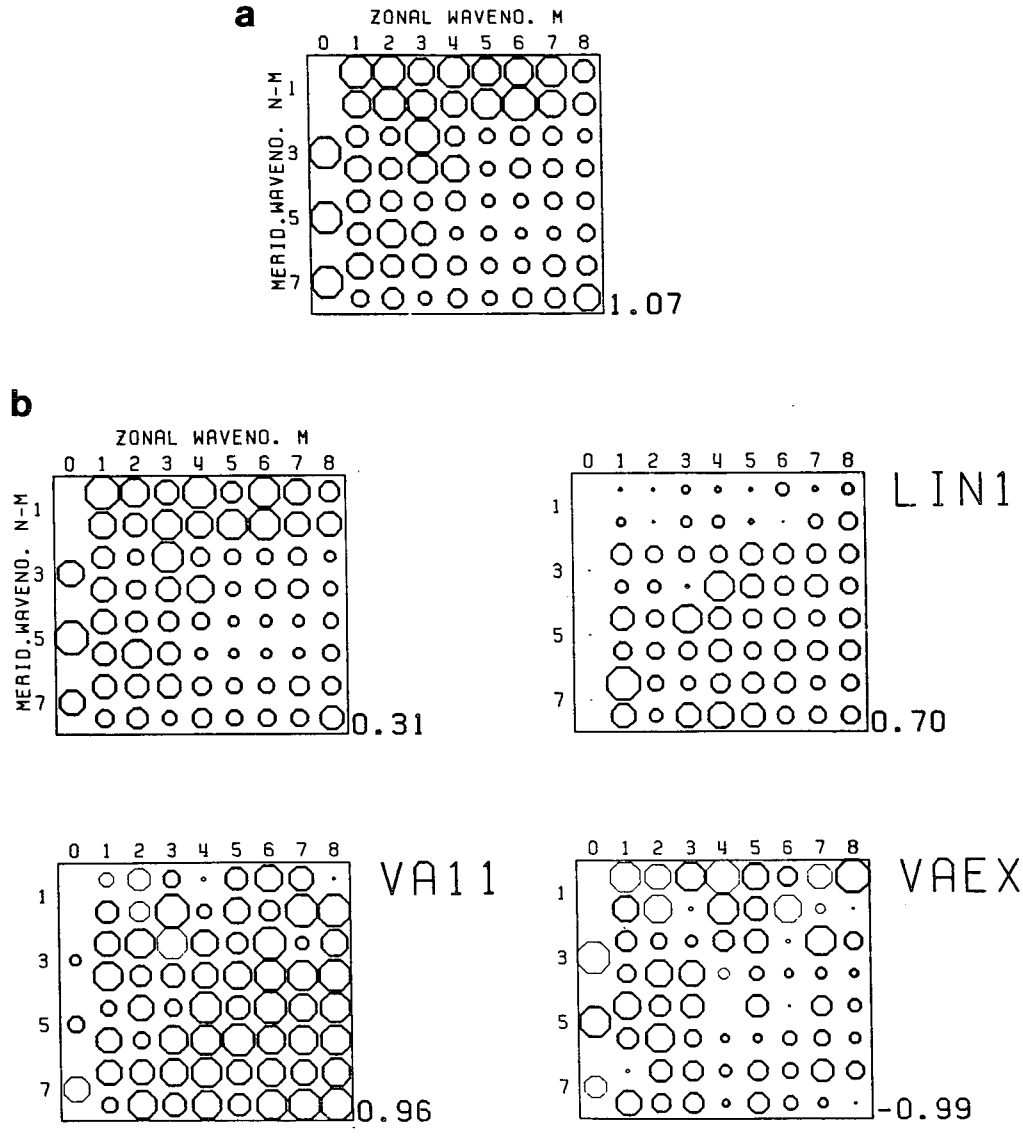

FIG. 13. (a) Wavenumber representation of the variance of the sum of the three predictors LIN1, VA11 and VAEX relative to the sum of their variances. (b) Wavenumber representation of the smallest eigenvalue λ (upper left panel) of the predictor correlation matrix at zero frequency and the corresponding coefficients h_j. The numbers represent the maximum value in each panel; thin octagons indicate negative values.

weakly affected by nonlinear interactions. Integrated over wavenumber space for medium and short periods we obtain about 50% explained variance with our model. However, at low frequencies both linear and nonlinear advection processes are poorly correlated with the long-term streamfunction tendencies. Only 27% observed variance is explained by the model for periods longer than two weeks. We have pointed out that our analysis must fail at low frequencies in the presence of only a little noise. In the limit of very low frequencies the streamfunction change represents (by definition) a small residual imbalance of all physical processes. However, we found that the imbalance between the three predictors included explicitly in the model is still relatively large, especially for the large scales. We therefore conclude that the model deficiency must be attributed to missing proces, such as slowly changing boundary conditions or the nonlinear interactions with the synoptic scales smaller than $n = 15$.

Our result, that at all time scales the external nonlinear interactions (VAEX, TAEX) are of the same magnitude as the internal interactions (VA11, TA12), supports the hypothesis of Egger and Schilling that synoptic eddies have an impact on the long-term variability of the planetary flow. Their model predicts a geographically inhomogeneous distribution of low-frequency variance forced by nonlinear vorticity transfer from synoptic scales. For a direct comparison it would

be interesting to rerun our analysis in physical space to determine the geographical distribution of the long-term variability and low-frequency forcing.

Acknowledgments. The author wishes to thank K. Hasselmann for many helpful discussions and comments on the manuscript, and H. Kruse for providing the streamfunction data and continual support during the progress of this study.

REFERENCES

Ahlquist, J. E., 1982: Normal mode global Rossby waves: Theory and observations. *J. Atmos. Sci.*, **39,** 193–202.

Bruns, T., 1985: Eine diagnostische untersuchung der Beiträge interner quasi-geostrophischer prozesse zur grossräumigen atmosphärischen variabilität. Dissertation, Universität Hamburg, 100 pp.

Baines, P. G., and J. S. Frederiksen, 1978: Baroclinic instability on a sphere in two layer models. *Quart. J. Roy. Meteor. Soc.*, **104,** 45–68.

Charney, J. G., and J. G. DeVore, 1979: Multiple flow equilibria in the atmosphere and blocking. *J. Atmos. Sci.*, **36,** 1205–1216.

——, and D. M. Straus, 1980: Form-drag instability, multiple equilibria and propagating planetary waves in baroclinic, orographically forced, planetary wave systems. *J. Atmos. Sci.*, **37,** 1157–1176.

Deland, R. J., 1964: Travelling Rossby waves. *Tellus,* **16,** 271–273.

Eliasen, E., and B. Machenhauer, 1965: A study of the fluctuations of the atmospheric planetary flow patterns represented by spherical harmonics. *Tellus,* **17,** 220–238.

——, and ——, 1969: On the observed large scale atmospheric wave motions. *Tellus,* **21,** 149–165.

Egger, J., 1981: Stochastically driven large-scale circulations with multiple equilibria. *J. Atmos. Sci.*, **38,** 2606–2618.

——, and H.-D. Schilling, 1983: On the theory of the long-term variability of the atmosphere. *J. Atmos. Sci.*, **40,** 1073–1085.

Fraedrich, C., and T. Dümmel, 1983: On single station forecasting: The geopotential height, its vertical and times structure and 500 mb ARMA-prediction. *Contrib. Atmos. Phys.*, **56,** 221–239.

Frederiksen, J. S., 1978: Instability of planetary waves and zonal flows in two-layer models on a sphere. *Quart. J. Roy. Meteor. Soc.*, **104,** 841–872.

Hayashi, Y., 1971: A generalized method of resolving disturbances into progressive and retrogressive waves by space Fourier and time cross-spectra analyses. *J. Meteor. Soc. Japan,* **49,** 125–128.

——, 1982: Space–time spectral analysis and its applications to atmospheric waves. *J. Meteor. Soc. Japan,* **60,** 156–171.

Jenkins, G. M., and D. G. Watts, 1968: *Spectral Analysis and its Applications.* Holden-Day, 525 pp.

Kruse, H., 1983: A statistical–dynamical low-order spectral model for tropospheric flows. Ph.D. dissertation, *Hamburger Geophys. Einzelschr.*, **A59,** Wittenborn Söhne, Hamburg, 141 pp.

——, 1985: Investigation of processes governing the large-scale variability of the atmosphere using low-order barotropic spectral models as a statistical tool. *Tellus* (in press).

Madden, R., 1979: Observations of large-scale traveling Rossby waves. *Rev. Geophys. Space Phys.*, **17,** 1935–1949.

——, and P. Julian, 1972: Further evidence of global scale 5-day pressure waves. *J. Atmos. Sci.*, **29,** 1464–1469.

Reinhold, B. B., and R. T. Pierrehumbert, 1982: Dynamics of weather regimes: Quasi-stationary waves and blocking. *Mon. Wea. Rev.*, **110,** 1105–1145.

Smith, S. M., H. W. Menert and G. Sharman, 1965: Worldwide ocean depth and continental elevations averaged for areas approximately 1-degree squares of latitude and longitude. Scripps Institution of Oceanography, Ref. Rep. 65-8.

Speth, P., and E. Kirk, 1981: Representation of meteorological fields by spherical harmonics. *Meteor. Rundsch.*, **34,** 5–10.